Journal of Achievements in Materials and Manufacturing Engineering
VOLUME 47
ISSUE 1
July
2011

Laser surface alloying of sintered stainless steels with SiC powder

Z. Brytan*, L.A. Dobrzański, W. Pakieła
Division of Materials Processing Technology, Management and Computer Techniques in Materials Science, Institute of Engineering Materials and Biomaterials, Silesian University of Technology, ul. Konarskiego 18a, 44-100 Gliwice, Poland
* Corresponding author: E-mail address: zbigniew.brytan@polsl.pl

Received 20.05.2011; published in revised form 01.07.2011

Manufacturing and processing

ABSTRACT

Purpose: The goal of this study is to investigate effects of laser surface alloying with SiC powder on microstructural changes and properties of vacuum sintered austenitic X2CrNiMo17-12-2, ferritic X6Cr13 and duplex X2CrNiMo22-8-2 stainless steels.
Design/methodology/approach: Surface modification of sintered stainless steels was carried out by laser surface alloying with SiC powder using high power diode laser (HPDL). The influence of laser alloying conditions, the laser beam power (between 0.7 and 2.1 kW) at constant scanning rate on the width of alloyed surface layer and penetration depth were studied. The resulting microstructure in laser alloyed surface layer was examined using light and scanning electron microscopy. Phase composition was determined by the X-ray diffraction method. The microhardness results of modified surface layer were also studied.
Findings: The alloyed surface layer has a fine dendritic microstructure with iron-chromium carbides precipitations. The surface layer was enriched in silicon and carbon that produced microstructural changes and resulting microhardness increase. Beside studied stainless steels the duplex one revealed highest hardening effect by laser alloying with SiC powder, where related microhardness was about 500-600 HV.
Practical implications: Laser surface alloying with SiC powder can be an efficient method of surface layer hardening of sintered stainless steels and produce significant improvement of surface layer properties in terms of hardness and wear resistance.
Originality/value: Application of high power diode laser can guarantee uniform heating of treated surface, thus uniform thermal cycle across processed area and uniform penetration depth of alloyed surface layer.
Keywords: High Power Diode Laser (HPDL); Laser surface alloying; Stainless steel; Silicon carbide

Reference to this paper should be given in the following way:
Z. Brytan, L.A. Dobrzański, W. Pakieła, Laser surface alloying of sintered stainless steels with SiC powder, Journal of Achievements in Materials and Manufacturing Engineering 47/1 (2011) 42-56.

1. Introduction

The comprehensive studies on the influence of surface laser treatment of various austenitic grades have shown the improvement of their intergranular, pitting and cavitation erosion resistance and also wear resistance after laser surface melting. Laser surface remelting was successfully applied to restore localized corrosion resistance in sensitized and in cold-worked and sensitised stainless steel. Further improvement of surface layer in respect of wear resistance can be obtained by alloying of stainless steel with hard particles such as carbides Cr_3C_2 in aim to locally reinforce the surface of austenitic stainless steel. The surface hardening of austenitic stainless steel can be achieved with different routs i.e. the incorporation of hard particles of TiC,

SiC, WC and carbon alloying in order to form carbides as well as alloying with Si_3N_4 nitrides and borides and their mixes or elements such as Mo resulting in the modification of their resistance to pitting or intergranular corrosion and stress corrosion cracking. Kwok et al. [6] studied influence of various elements (Co, Ni, Mn, C, Cr, Mo, Si) and compounds (AlSiFe, Si_3N_4, NiCrSiB) on austenitic stainless steel microstructure and properties after laser surface melting. The highest improvement in corrosion resistance achieved with Si and Si_3N_4 powders. The laser alloying of AISI 316 stainless steel with Al-Si powder also considerably improves cavitation erosion resistance and hardness [1-7].

Laser surface allying using HPDL laser is well established method of surface properties improvement for many materials including tool steels [8], magnesium alloys [9], titanium alloys [10], aluminium alloys [11] and many others [12,13].

The stainless steel is constantly very inserting for scientist regarding development of new alloys as well as surface modification by conventional treatments and methods [14-17].

The sintered stainless steels are an important structural material for brand spectrum of applications and branches. One of the most important is automotive industry, but other like household appliances, electromechanical devices and precision devises are also frequently consumers of that materials. The production of sintered parts form stainless steels is well known and industrialized [18]. The sintered stainless steels are widely used thank to their high corrosion resistance, but due to low hardness their terminological properties are still very weak. Laser surface remelting of PM austenitic stainless steel may result in the improvement of overall material properties in surface layer due to density reduction and microstructure refinement, therefore the mechanical and corrosion performance will increase [19]. Moreover, laser surface alloying with chromium may extra enrich the chemical composition thus enhance its properties and corrosion resistance and extend the range of possible applications. The laser surface alloying of single phase wrought austenitic stainless steel with ferrite forming element like Cr can produce duplex (austenite + ferrite) microstructure in surface layer thus increasing hardness and corrosion resistance of surface [20].

The sintered stainless steels of different microstructure (austenitic, ferritic and duplex) were laser alloyed with SiC powder. The influence of laser alloying processing conditions on materials properties was evaluated.

2. Experimental procedure

2.1. Substrate material

Three different sintered stainless steels were produced and investigated: austenitic, ferritic and duplex stainless steel with compositions presented in Table 1. For powder preparation the austenitic stainless steel powder 316LHD and ferritic 410LHD of Hoeganes with particle size of <150 µm were used. The duplex sintered stainless steel was obtained by addition of single element powders such as FeCr, Ni, Mo and Cu powder in right quantity to the master alloy of ferritic 410LHD powder to obtain the chemical composition similar to duplex one. The manufacturing procedure of sintered stainless steel was well described in the paper [26]. During preparation of stainless steel powders the Acrawax was used as a lubricant in the quantity of 0.65 wt.%. Premixes were prepared in Turbula mixer for 20 min. and then uniaxially compacted in specimens of 10×10×55 mm at 700 MPa. The de-waxing process was performed at 550°C for 60 minutes in a nitrogen atmosphere. Samples were then sintered in a vacuum furnace with Ar backfilling at temperature 1250°C for 60 min. During the sintering cycle a solution annealing at 1050°C/1h was done and then the rapid cooling under pressure of 0.6 MPa of nitrogen was applied.

2.2. Laser surface alloying

The laser surface alloying was performed using Rofin DL 020 high power diode laser (HPDL) with rectangular laser beam spot at argon atmosphere with the following laser parameters: radiation wavelength 808±5 nm, beam output power (continuous wave) 2300 W, beam focal length 82/32 mm, laser beam spot dimension 1.8-6.8 mm, power density range in the laser beam plane 0.8-36.5 kW/cm^2. The laser treatment was conduced at 0.7, 1.4 and 2.1 kW of laser beam power and constant scanning speed rate of 0.5 and 0.3 m/min.

The alloyed surface layers on sintered stainless steel were produced as single stringer beads, the laser beam was focused on the top of specimens. The long side of laser beam spot was set perpendicularly to the alloying direction. The laser beam was guided along longer side (55 mm) of specimens, the side compatible with their pressing direction.

The surface of sintered stainless steel was covered with 0.l mm thin layer of SiC powder applied on surface in form of paste prepared as a mixture of inorganic sodium glass in proportion 30% glass and 70% SiC powder.

Second approach consisted in the special mechanical working of sample surface, where on specimens surface two or three parallel grooves, deep for 0.5 and 1.0 mm of triangular shape (with angle of 45°) were machined. The grooves were located along sample axis and distance between them was ca. 1.0 mm. Such prepared grooves were filled with pure SiC powder.

2.3. Materials characterization

Microstructure observations and geometrical characteristics of weld bead were carried out in the light and scanning electron microscope (SEM) with the EDS probe.

The evaluation of phase composition was made using X-ray diffractometer with the filtered copper lamp rays at acceleration voltage of 45 kV and heater current of 40 mA. The measurements were made in diffraction angle from 30 to 130° of 2θ. The x-ray scan was performed parallel to alloying direction.

The Vickers microhardness $HV_{0.1}$ was measured on the cross-section of alloyed surface in the FM-AKS 9000 of Future-Tech automated microhardness tester and a depth profile of the microhardness was determined.

Abrasion behaviours have been tested using pin-on-plate method, where hardened steel ball was reciprocally moved along the surface. The wear test was evaluated basing on the confocal images of produced wear track and wear volume was calculated.

Table 1.
The nominal chemical composition of sintered stainless steels powders used in investigations

Powder designation		Elements concentration, wt.%								
EN 10088 corresponding grade	Manufacturer designation	Cr	Ni	Mo	Si	Mn	C	N	S	Fe
X2CrNiMo17-12-2	316 LHD	16.2	12.3	2.2	0.9	0.10	0.019	0.05	0.006	bal.
X6Cr13	410 LHD	11.9	0.15	-	0.8	0.08	0.009	0.05	0.03	bal.
X2CrNiMo22-8-2	-	22.72	8.10	2.00	0.70	0.60	0.03	-	-	bal.

3. Results and discussion

The sintered stainless steel shows density of between 7.2-7.3 g/cm^3 and open porosity of about 5% and ca. 92% of theoretical density. The microstructure of austenitic stainless steel prior the laser treatment was composed of austenitic grains with presence of some twinned grains. The ferritic stainless steel shows regular grains of ferrite while duplex microstructure was composed of uniform distributed ferritic and austenitic grains. Applied sintering cycle in vacuum followed be rapid cooling directly from sintering temperature enabled correct duplex microstructure formation without precipitations of intermetallic phases.

The dimensions of laser alloyed zone change with the applied laser beam power. The increase of the laser beam power resulted in light widening of surface size of remelting zone in the range of 5.0-6.0 mm when using laser beam power of 1.4 and 2.1 kW (Fig. 1a). Application of laser beam power of 0.7 kW was not sufficient to remelt the surface, thus no process of alloyed layer was observed. The penetration depth of alloyed layer increased too with higher laser beam power. Beside evaluated sintered stainless steels the austenitic X2CrNiMo17-12-2 shows highest penetration depth ca. 0.9 mm, while for duplex it was ca. 0.6 mm and only 0.2-0.3 for ferritic stainless steel (Fig. 1b).

It was previously reported by authors [19,20] that sintered austenitic stainless steel remelted in similar conditions shows maximal penetration depth of 1.0 mm, so the presence of alloying paste on samples surface considerably decreased the maximal possible penetration depth. Pre-coated thin layer (0.1 mm) of SiC past on the sample surface reflects laser beam radiation and lowers the penetration depth due to high reflectance loss of the incident laser beam that also depends on its colour and roughness. Moreover sintered stainless steels shows lower penetration depth when compared to the wrought one [20] due to porosity that retains heat and acts as an insulator and thus decreases thermal conductivity of material.

Surface pre-coated with SiC powder after laser remelting shows non-uniform surface topography. Depending on laser conditions surface has non regular remelted zone and only when using high laser energy the surface quality can be acceptable. The cross-sectional views of sintered stainless steels surface layer alloyed with SiC powder in form of pre-coated paste were presented in Fig. 2.

Generally in aim to obtain properly remelted surface layer, when using pre-coated paste of SiC powder at constant scanning speed of 0.5 m/min the laser beam power should be as high as possible, in case of studied conditions 2.1 kW should be used.

Stainless steels surfaces prepared as machined grooves (2 or 3 groves) of different depths (0.5 or 1.0 mm) showed that the best results in term of quality of surface layer were obtained for 3 groves and their depth of 0.5 mm (Fig. 3). General conclusion can be made in this point of discussion that surface with grooves filed with alloying powder SiC ensure better remelting surface quality than surface covered with powder paste that acts as the barrier for laser radiation and finely lowering possible penetration depth and overall laser energy reaching surface.

In case of samples where in surface grooves were machined and then filled with SiC powder the overall penetration depth was higher for all alloyed stainless steels. As in the previous case, austenitic stainless steel shows the highest penetration depth (Fig. 4) also for this kind of powder deposition.

a)

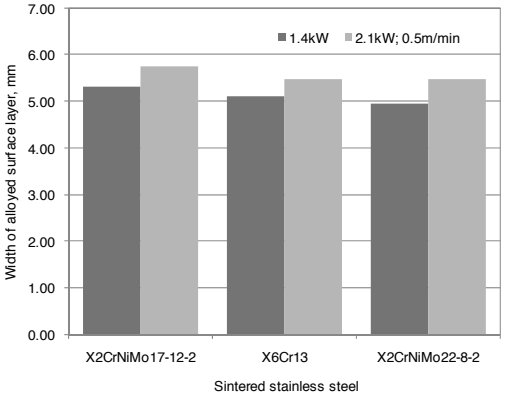

b)

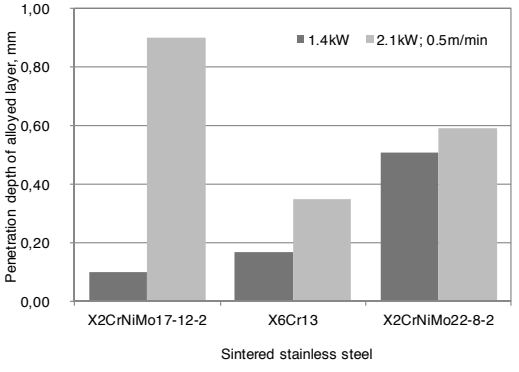

Fig. 1. Geometrical characterization of alloyed layer, a) width and b) penetration depth of surface pre-coated with SiC powder paste and laser processed

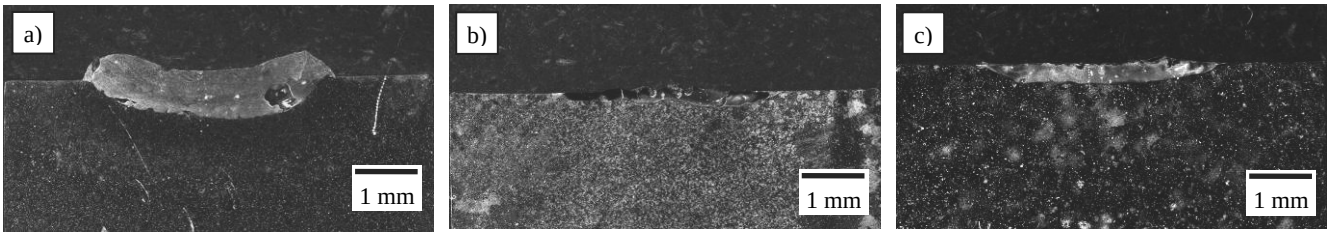

Fig. 2. The surface layer cross section of stainless steel, respectively a) austenitic, b) ferritic and c) duplex stainless steel alloyed with SiC powder in form of pre-coated layer at laser beam power of 2.1 kW and scanning speed 0.5 m/min

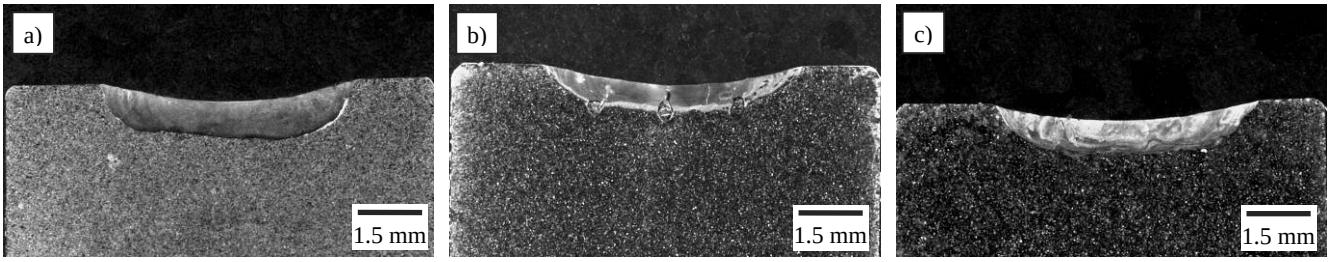

Fig. 3. The surface layer cross section of stainless steel, respectively a) austenitic (2 grooves), b) ferritic (3 grooves) and c) duplex stainless steel (2 grooves) alloyed with SiC powder, that filled surface grooves, at laser beam power of 2.1 kW and scanning speed 0.3 m/min

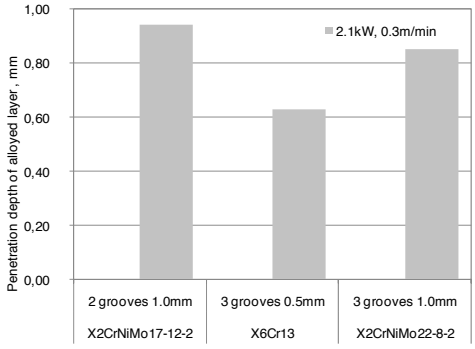

Fig. 4. Penetration depth of remelted layer alloyed with SiC powder, surface with grooves at laser beam power of 2.1 kW and scanning speed 0.3 m/min

Stainless steels surfaces prepared with pre-coated paste shows lover quality than prepared as machined grooves. The way of SiC deposition on the surface influences the quantity of remelted material and dilution ratio. Regarding the surface quality when SiC was deposited as pre-coated paste it was satisfactory for sintered ferritic (Fig. 5a) and austenitic stainless steels after laser alloying, but in case of duplex stainless steel (Fig. 5b) and low laser beam powers the superficial porosities where drastically higher. This effect was completely eliminated in case of remelting surface with machined grooves filled with SiC powder (Fig. 6).

The surface of stainless steels alloyed with SiC shows black dust deposits after laser process that is probably the burned carbon particles. This black deposit is easily removable with standard cleaning method. After cleaning the surface has a silver metallic shine (Fig. 6), and weld bead of alloyed layer is uniform, flat and smooth without any visible undercuts or superficial cracks.

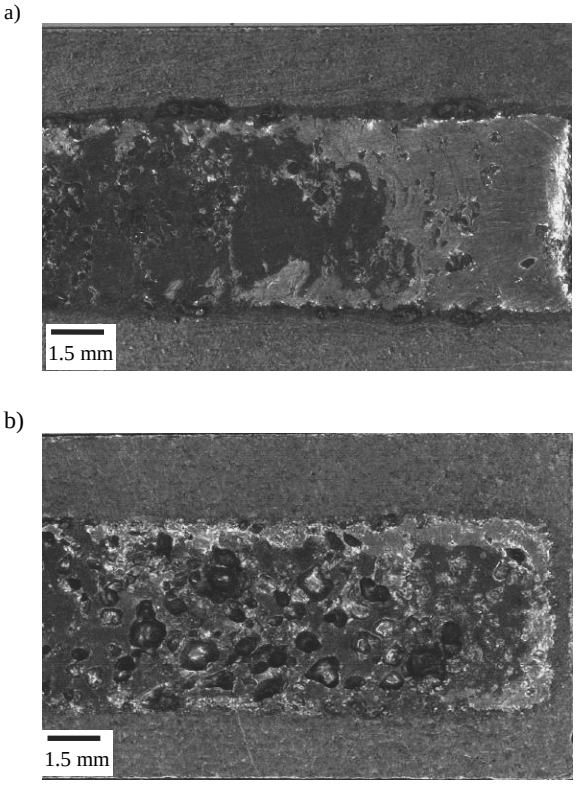

Fig. 5. Surface layer of sintered stainless steels alloyed with SiC powder in form of pre-coated paste of 0.1 mm, laser beam power 2.1 kW, scanning speed 0.5 m/min, a) sintered ferritic stainless steel X6Cr13, b) duplex stainless steel X2CrNiMo22-8-2

a)

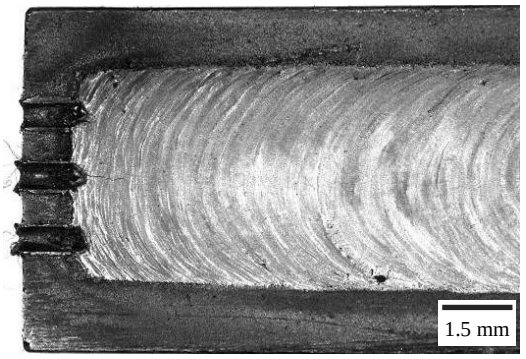

b)

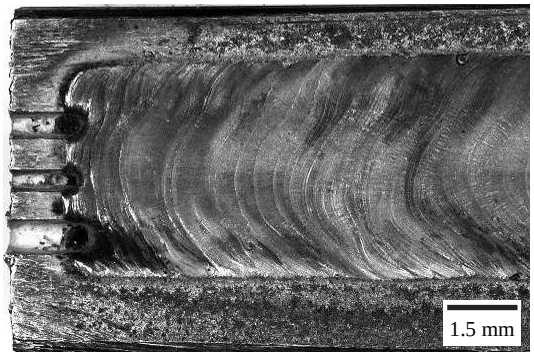

Fig. 6. Surface layer of sintered stainless steels alloyed with SiC powder, surface with machined grooves, a) austenitic stainless steel X2CrNiMo17-12-2, 3 grooves of 0.5 mm and b) duplex stainless steel X2CrNiMo22-8-2, 3 grooves of 0.5 mm

Laser alloyed stainless steels (Figs. 7-9) shows fine cellular dendritic microstructures, where during solidification Si and some amounts of C dissolve in the steel matrix. The steel matrix supersaturation in silicon and carbon causes silicides and carbides precipitations. The formation of different iron silicides, such as Fe_2Si, Fe_3Si, Fe_5Si_3 and FeSi, based on the Si content in the system, has also been reported in the literature [21-25]

The microstructure of austenitic stainless steels remelted with SiC powder in form of pre-coated paste shows dendritic structure (Figs. 7a, 7b) resulting from the rapid solidification process. Microstructure is composed of primary dendrites of austenite phase (Fig. 7a) and interdendritic lamellar eutectics of austenite and carbides M_7C_3 (M = Cr, Fe) (Fig. 7b). Similar eutectic structure consisting of dendrites of austenite with M_7C_3 carbides in the interdendritic areas was reported in literature [1,3,25] in austenitic stainless steel AISI 304 and 316L alloyed with SiC paste deposited by brushing.

The ferritic stainless steel (Figs. 8a, 8b) shows fine dendritic structure where slightly bigger dendrites of elongated shape and oriented along direction of heat transfer on the border between parent material and remelted zone can be observed (Fig. 8a). The central zone of remelted layer is composed of very fine and regularly distributed dendrites and precipitations of silicides and flower-shaped carbides (Fig. 8b) which predominate at the top of alloyed layer. The microstructure consists of M_7C_3 carbides surrounding the eutectic phase that are composed of rich Fe and Si The X-ray analyses (Fig. 9) revealed that dissolution of SiC in stainless steel matrix and enrichment in Si and C produced formation of cubic iron silicon Fe_3Si, carbon iron silicon $C_{0.12}$ $Fe_{0.79}$ $Si_{0.09}$ and some Fe_2Si phase as well as silicon carbide SiC of rombohedral lattice and M_7C_3 type carbide. Laser surface alloying with SiC performed on medium carbon steel, reported by Thawari [24] revealed similar phases which formation depend of the extent of dilution of the alloyed layer by iron from parent metal.

The duplex stainless steel (Fig. 10) after SiC alloying shows the finest dendritic structure. The rapid solidification in laser surface alloying process connected with SiC alloying caused increased ferrite content in duplex microstructure. The top layer is highly enriched in carbon than center one, so higher concentration of carbides precipitations occurred in this zone. Basing on the X-ray analysis (Fig. 11) following phases have been confirmed: austenite, ferrite, possibly martensite, carbides M_7C_3 type, SiC phase and silicon rich phases as FeSi, Fe_3Si as well as $C_{0.12}$ $Fe_{0.79}$ $Si_{0.09}$ phase.

a)

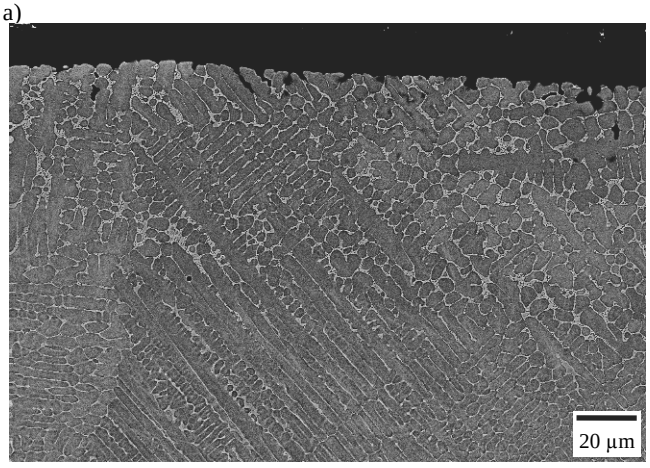

b)

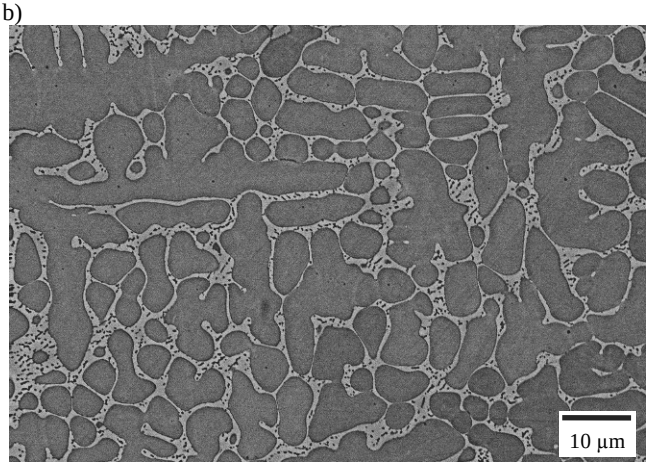

Fig. 7. Microstructure of sintered austenitic stainless steel X2CrNiMo17-12-2 alloyed with SiC in form of pre-coated paste at laser power of 2.1 kW, scanning speed rate 0.5 m/min, a) the top layer of remelting zone and b) magnification in centre zone

a) b)

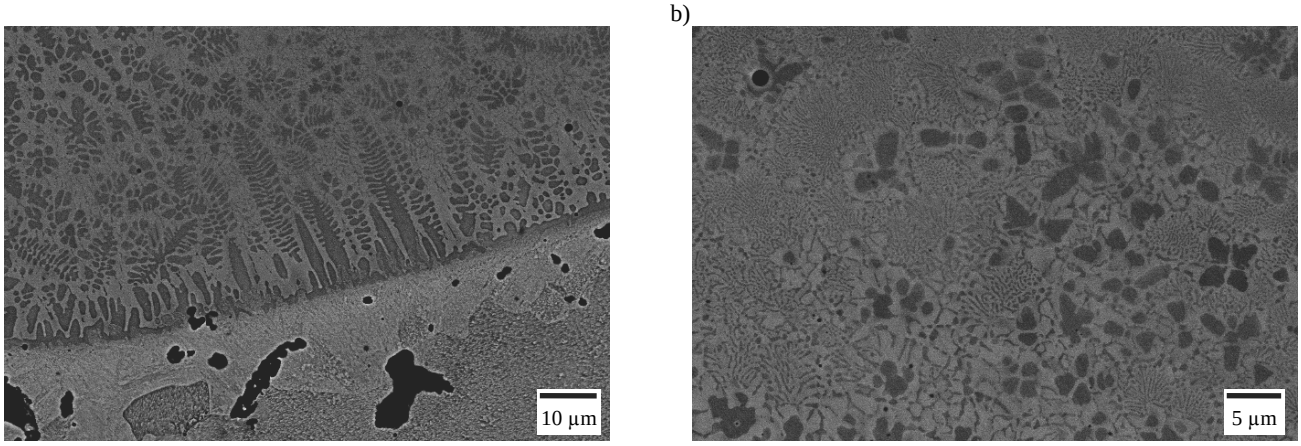

Fig. 8. Microstructure of sintered ferritic stainless steel X6Cr13 alloyed with SiC in form of pre-coated paste at laser power of 2.1 kW, scanning speed rate 0.5 m/min, a) the border of alloyed layer and parent metal, b) magnification in the top layer

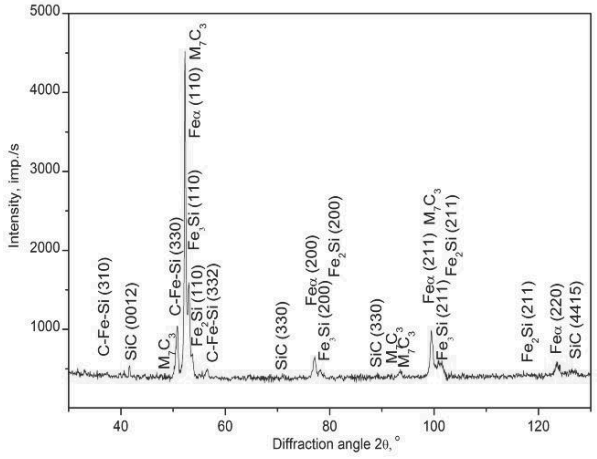

Fig. 9. The X-ray diffraction of sintered ferritic stainless steel X6Cr13 alloyed with SiC in form of pre-coated paste at laser beam power of 2.1 kW and scanning speed rate 0.5 m/min

a) b)

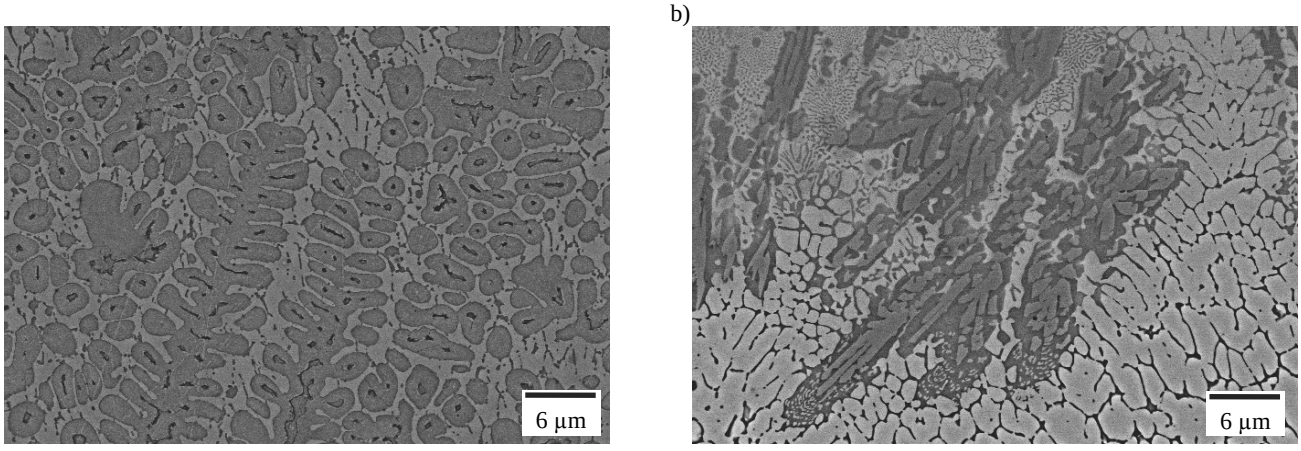

Fig. 10. Microstructure of sintered duplex stainless steel X2CrNiMo22-8-2 alloyed with SiC in form of pre-coated paste at laser beam power of 2.1 kW and scanning speed rate 0.5 m/min, a) the center of remelting layer and b) magnification in the top of remelted layer

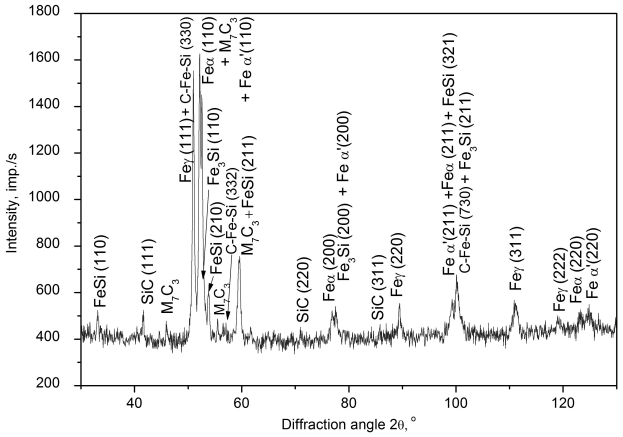

Fig. 11. The X-ray diffraction of sintered duplex stainless steel X2CrNiMo22-8-2 alloyed with SiC in form of pre-coated paste at laser beam power of 2.1 kW and scanning speed rate 0.5 m/min

Detailed analysis of alloyed layer of duplex stainless steel confirmed microstructure of M_7C_3 carbides surrounding the eutectic phase that are composed of rich Fe and Si (Fig. 12). The core of alloyed layer is composed of fine ferritic grains with clearly visible grains boundaries. The ferritic matrix consists of 22% Cr, 6% Ni and 7% Si. The top of alloyed layer is more inhomogeneous in terms of formed structure and presented phases. Table 2 shows results of EDS analysis in the zone of hexagonal carbide, where these carbides were surrounded by a matrix of eutectic carbides and austenite phase. The carbides contains ca. 50% Cr and 30% Fe, the austenitic phase shows 14% Cr and 9% Ni and ca. 9% of silicon, while the interdendritic eutectic structure 6% Si, 21% Cr, 6% Ni and 2% Mo. The medium concentration of silicon in alloyed layer was about 5.5% for applied laser beam power of 1.4 and 2.1 kW.

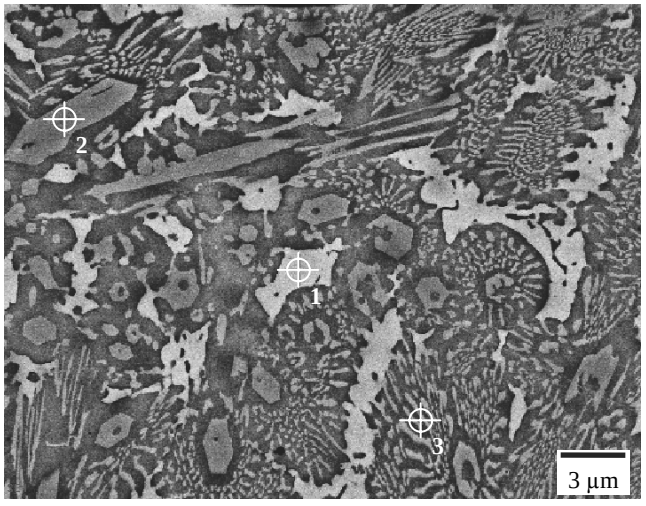

Fig. 12. Microstructure of sintered duplex stainless steel X2CrNiMo22-8-2 alloyed with SiC in form of pre-coated paste at laser beam power of 1.4 kW and scanning speed rate 0.5 m/min, magnification in the top of remelted layer

Table 2.
The EDS analysis in the surface layer, according to Fig. 12

	Analysis 1		Analysis 2		Analysis 3	
Phase	γ-austenite		carbide		eutectic region	
	wt. %	at. %	wt. %	at. %	wt. %	at. %
C	08.48	28.55	16.04	46.03	07.65	26.46
Si	09.01	12.97	00.78	00.96	06.18	09.14
Mo	05.57	02.35	02.30	00.83	02.09	00.90
Cr	14.51	11.28	50.13	33.24	21.35	17.06
Fe	53.02	38.38	29.22	18.04	56.53	42.05
Ni	09.41	06.48	01.53	00.90	06.21	04.39

Microstructures obtained for specimens with machined grooves (Figs. 13-15) were similar, but due to grooves and thus smaller quantity of alloyed SiC, the dilution rate was higher and obtained microstructures in all cases were more uniform.

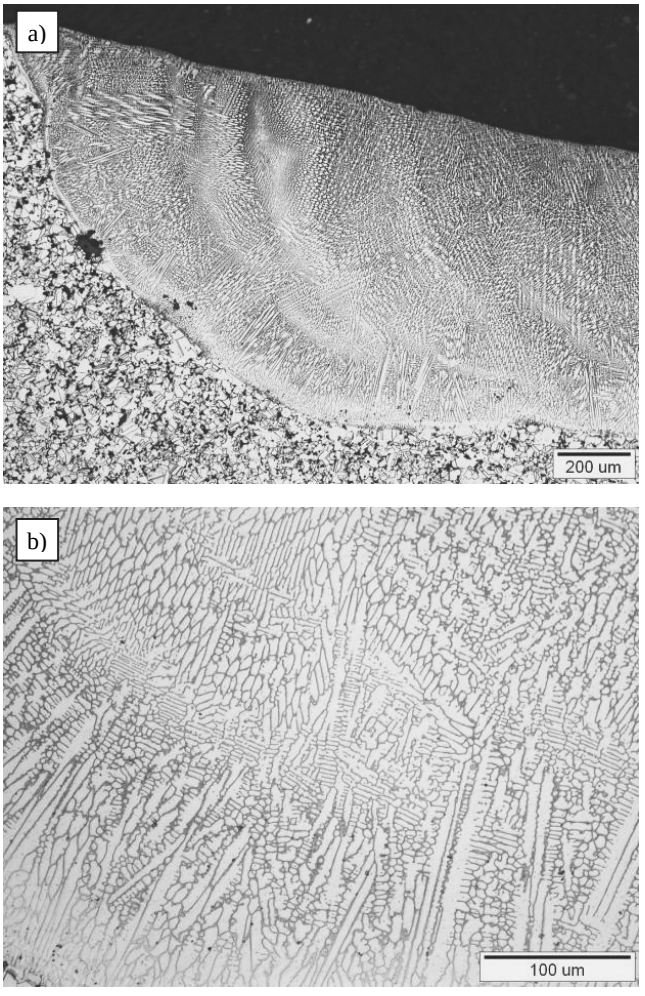

Fig. 13. Microstructure of austenitic stainless steel remelted with SiC powder, surface with 2 grooves, at laser beam power of 2.1 kW and scanning speed rate 0.3 m/min, a) the edge of remelting zone, b) magnification in central zone

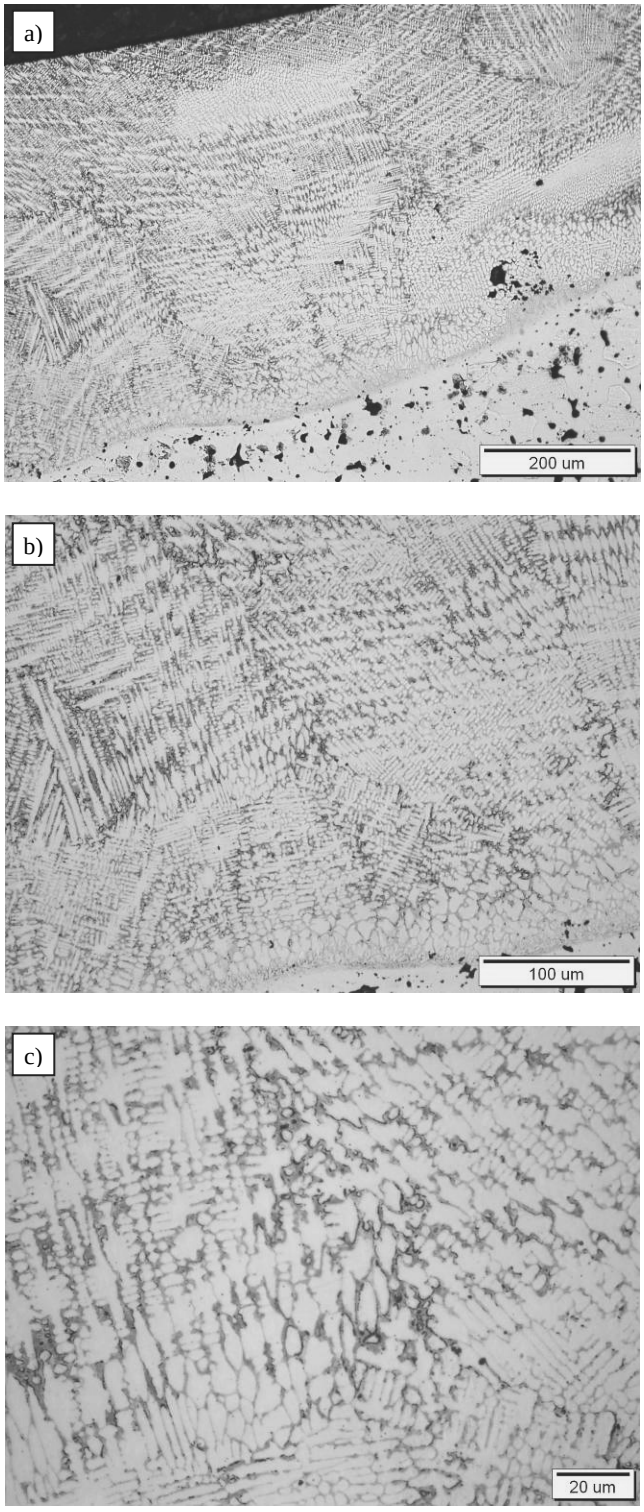

Fig. 14. Microstructure of ferritic stainless steel remelted with SiC powder, surface with 3 grooves, at laser beam power of 2.1 kW and scanning speed rate 0.3 m/min, a) the edge of remelting zone, b) central zone and c) magnification in central zone

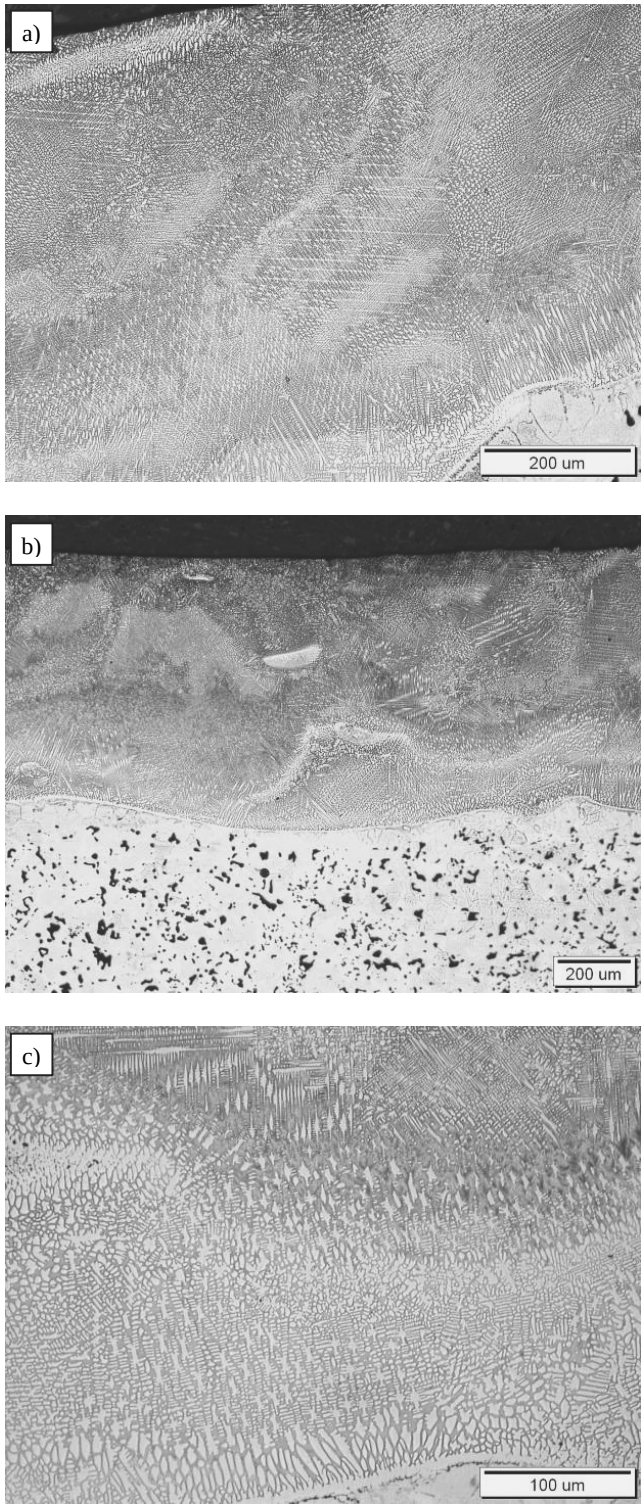

Fig. 15. Microstructure of duplex stainless steel remelted with SiC powder, surface with 3 grooves, at laser beam power of 2.1 kW and scanning speed rate 0.3 m/min, a) the edge of remelting zone, b) central zone and c) magnification in central zone

In order to determine temperature distribution during laser alloying of sintered stainless steels the infrared thermography was applied. The sequence of thermographic images was recorded using IR-camera (Figs. 16-18). The thermographic camera was placed 1 m from alloyed sample in order to provide observation in molten pool and at the surface of alloyed samples. Registered images were analyzed in dedicated software that allows identification of temperature values in selected point, determination of temperature profiles along registered picture, temperature distribution on the sample surface as well as heating and cooling time of processed material, etc.

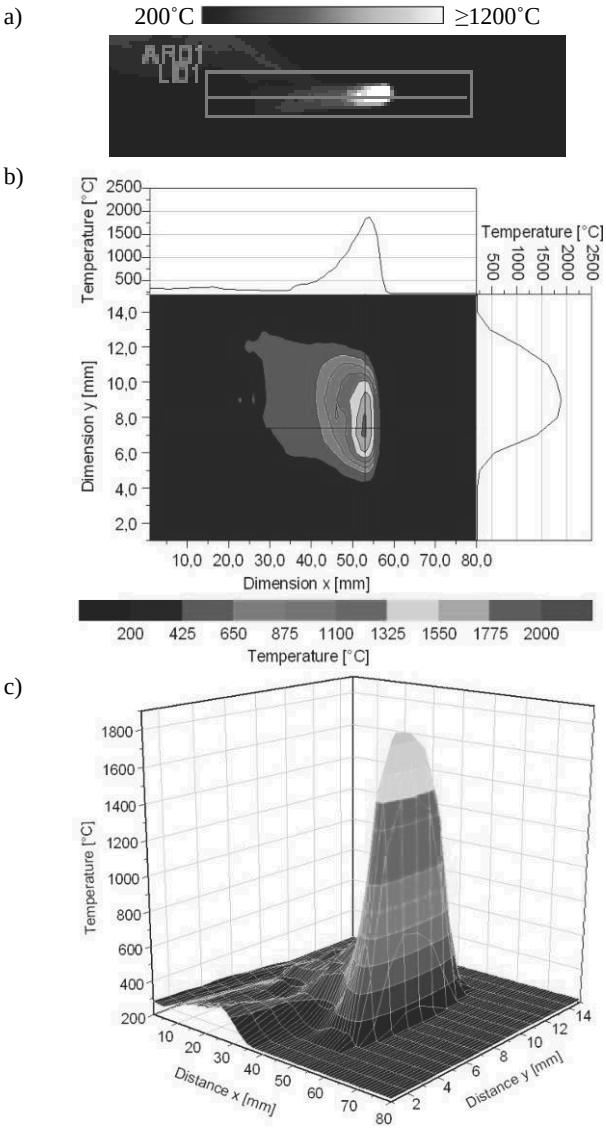

Fig. 16. Thermogram of molten pool during laser alloying with SiC of austenitic stainless steel X2CrNiMo17-12-2 at laser beam power of 0.7 kW, scanning speed rate 0.5 m/min, a) thermographic image, b) temperature distribution in AR01 area and along X and Y axis after 5 s, c) the spatial distribution of temperature from thermogram at image b)

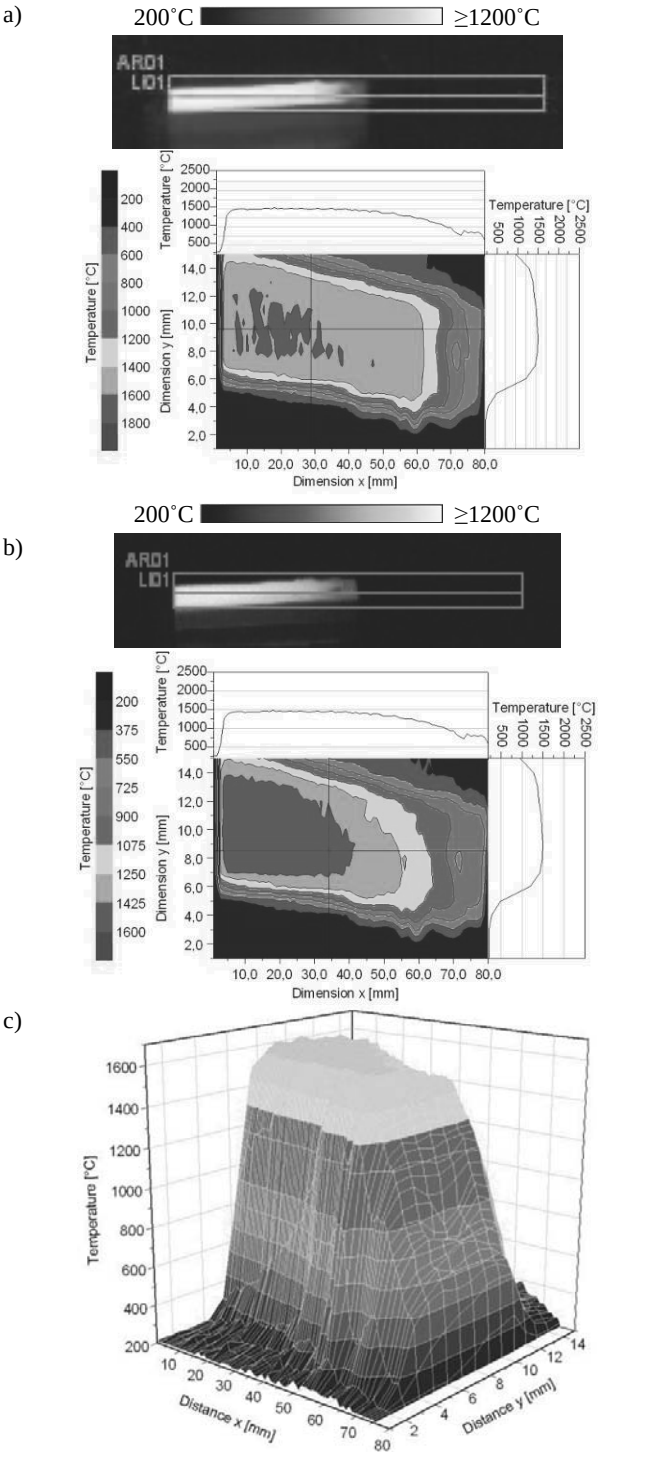

Fig. 17. Thermogram of molten pool during laser alloying with SiC of ferritic stainless steel X6Cr13 at laser beam power of 2.1 kW, scanning speed rate 0.5 m/min, a) thermographic image and temperature distribution in AR01 area and along X and Y axis after 8 s, b) after 11 s and c) the spatial distribution of temperature from image a)

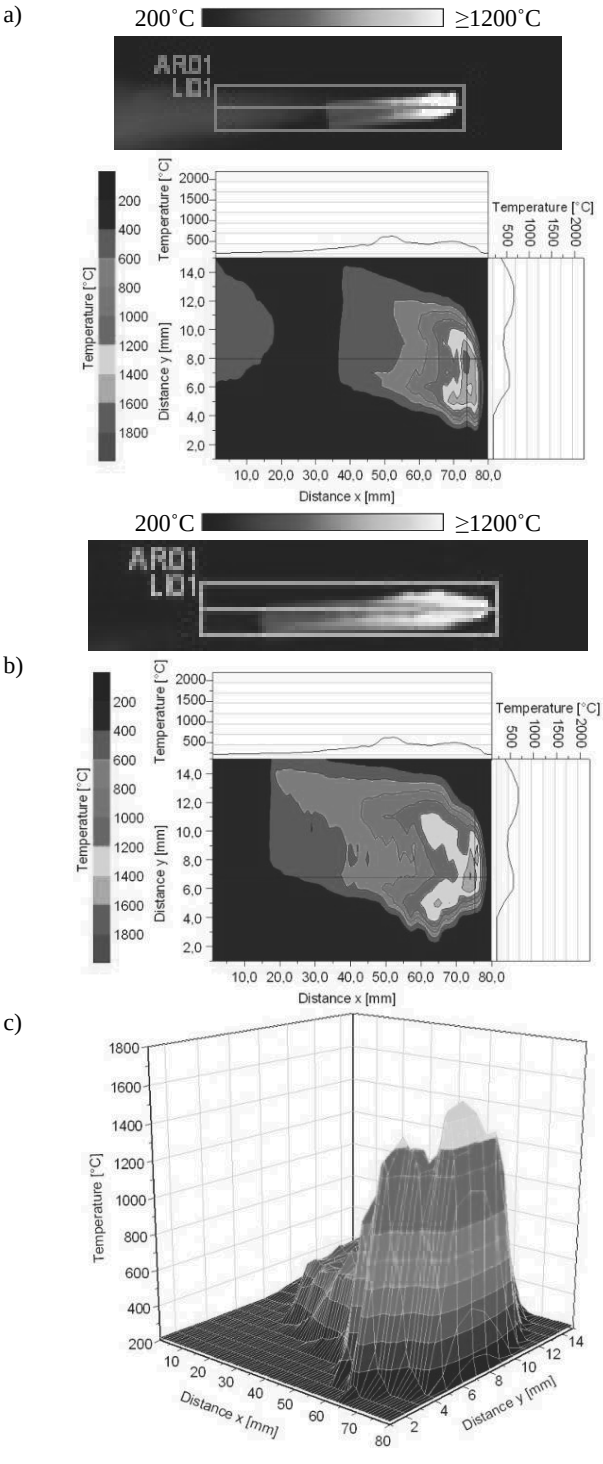

Fig. 18. Thermogram of molten pool during laser alloying with SiC of duplex stainless steel X2CrNiMoN22-8-2 at laser beam power of 1.4 kW, scanning speed rate 0.5 m/min, a) thermographic image and temperature distribution in AR01 area and along X and Y axis after 4 s, b) after 5 s and c) the spatial distribution of temperature from image a)

Analysis of thermographic images registered during laser alloying with SiC powder shows the smallest emission field of infrared radiation was observed for austenitic stainless steel X2CrNiMo17-12-2 (Fig. 16) and the largest one for ferritic (Fig. 17), while for duplex (Fig. 18) it was in the middle. This phenomenon is closely related to the thermo-physical properties of alloyed steel and alloying powder. Thermal conductivity and specific heat of silicon carbide particles in each case were the same and therefore infrared emission was mainly depended on thermal conductivity of alloyed substrate and applied laser beam power. The austenitic stainless steel comparing to ferritic and duplex alloy shows the lowest thermal conductivity, thus registered temperature of this sample was lower than for others alloys. Laser beam alloying is characterized by very high local power densities and high temperature gradients in molten pool, which even for low laser beam power of 0.7 kW shows temperatures above 1200°C. For this condition alloyed surface was not satisfactory in terms of obtained microstructures, what and can be explained that majority of laser energy was consumed for heating and melting and also vaporization of pre-coated SiC paste. The high temperature heat flux of evaporating paste products was visible along alloyed bead, e.g. during alloying at 1.4 kW (Fig. 18b), but when high laser beam power of 2.1 kW was applied majority of laser energy was consumed for melting pre-coated paste and simultaneously alloying the substrate.

In case of pre-coated paste theoretically higher quantity of alloying material can be remelted thus the higher hardness can be obtained due to not dissolved particles forming conglomerates on the surface layer and lower dilution rate producing higher quantity of carbides precipitations in the top of surface layers. Unfortunately application of pre-coated paste for applied laser conditions does not provide satisfactory surface quality. The microhardness depth profile of samples with pre-coated paste (Figs. 19-21) shows that not fully dissolved SiC particles, formed carbides and strong supersaturation in Si and C of the microstructure resulted in high microhardness. The austenitic stainless steel (Fig. 19) shows regular microhardness of about $400HV_{0.1}$ at maximum laser beam power. The hardening effect of SiC was strongest in case of ferritic stainless steel (Fig. 20) where microhardness increased to $1200HV_{0.1}$ for 1.4 kW. Such high microhardness in this case can be explained be high volume of precipitated carbides. Increasing laser beam power at constant powder content resulted in lower microhardness ca. $850HV_{0.1}$ for 2.1 kW, due to higher dissolution of substrate material and thus higher dilution ratio. The same mechanism occurred in duplex stainless steel (Fig. 21), where maximum hardness of $1000HV_{0.1}$ was obtained for 1.4 kW, while for 2.1 kW it was $600HV_{0.1}$.

The SiC alloyed surfaces with machined grooves shows lower microhardness (Figs. 22-24), but more uniform distribution of obtained microhardness at the penetration depth. Lower hardness of such layers is caused be higher dilution ratio and lower microhardness of dendritic structure that predominated at this laser alloying conditions. Beside studied variants of machined grooves (2 or 3) and their depth (0.5 or 1.0 mm), the layer with 2 grooves of 1.0 mm gives the same results as 3 groves of 0.5 mm (Fig. 22). Optimal results in term of surface quality, lack of cavities, uniform shape and smooth surface layer was obtained for 3 groves of 0.5 mm depth, what can be explained by high dilution ratio and therefore easier dissolution of the SiC particles.

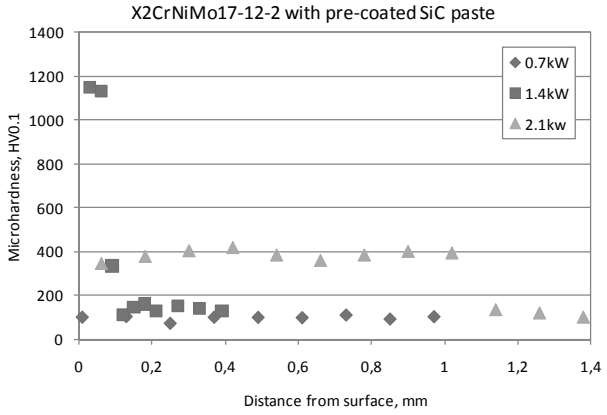

Fig. 19. Microhardness depth profile of austenitic stainless steels X2CrNiMo17-12-2 alloyed with SiC as pre-coated paste at varied laser beam powers

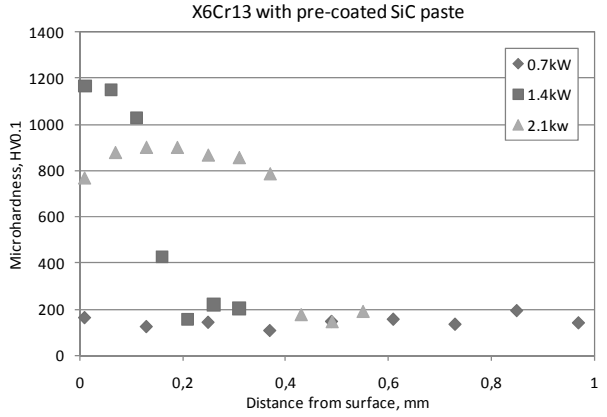

Fig. 20. Microhardness depth profile of ferritic stainless steels X6Cr13 alloyed with SiC as pre-coated paste at varied laser beam powers

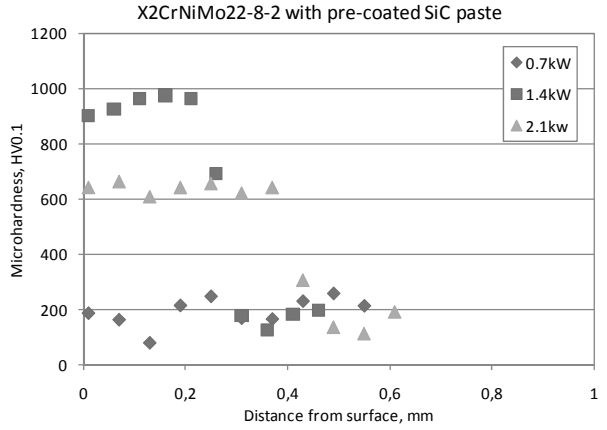

Fig. 21. Microhardness depth profile of duplex stainless steels X2CrNiMo22-8-2 alloyed with SiC as pre-coated paste at varied laser beam powers

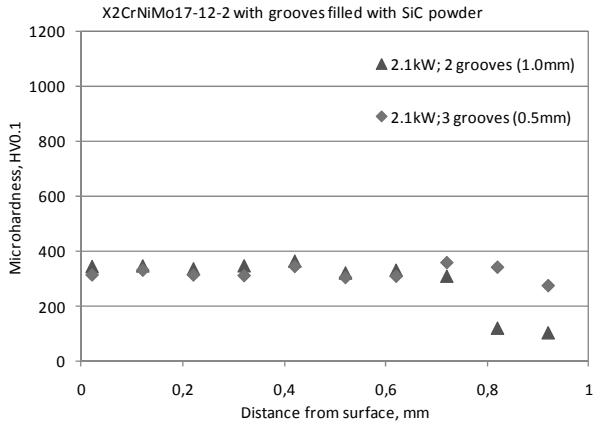

Fig. 22. Microhardness depth profile of austenitic stainless steels X2CrNiMo17-12-2 alloyed with SiC, surface with grooves at varied laser beam powers

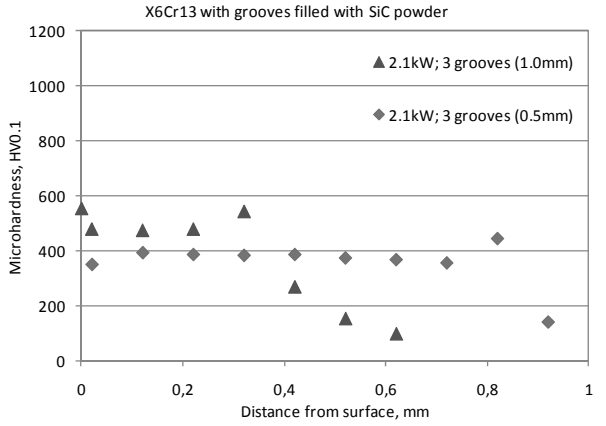

Fig. 23. Microhardness depth profile of ferritic stainless steels X6Cr13 alloyed with SiC, surface with grooves at varied laser beam powers

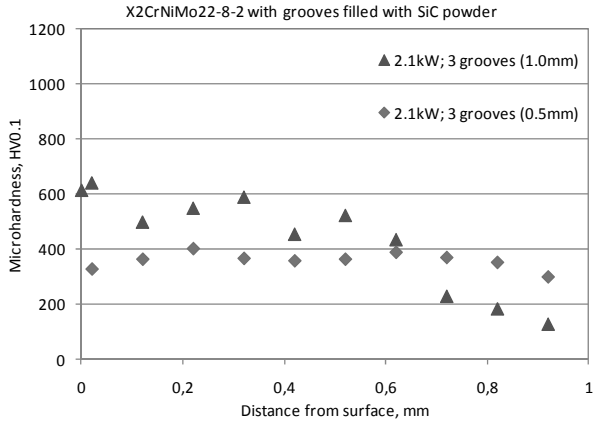

Fig. 24. Microhardness depth profile of duplex stainless steels X2CrNiMo22-8-2 alloyed with SiC, surface with grooves at varied laser beam powers

The abrasion wear behavior of laser alloyed layers was evaluated by simple tribological test similar to pin-on-plate test where loaded hardened steel ball was used as pin. The wear resistance was evaluated after constant value of cycles and then obtained wear track was measured using confocal microscopy. The wear track was measured in three axes x, y and depth z (Fig. 25) and then the wear volume was calculated taking into account rounded shape o wear track corresponding to ball diameter. Measured wear volume of not alloyed samples was much higher than that of any other tested samples. The improvement in wear resistance was observed in case of alloyed samples with machined grooves of 1.0 mm and more in samples with 3 grooves of 0.5 mm depth that obtained highest wear resistance among tested alloys (Fig. 26). The laser alloying with SiC powder in all cases can reduce even double the wear volume when compared to not alloyed surface.

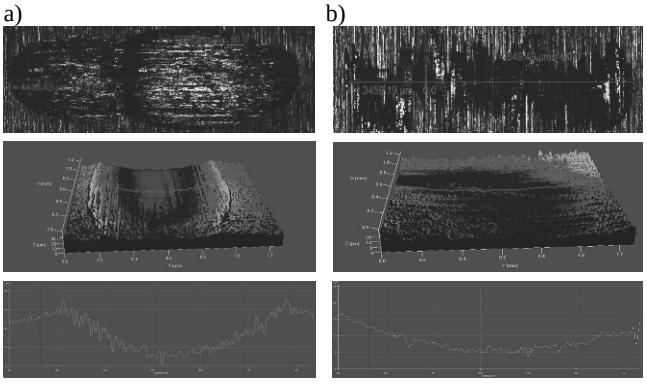

Fig. 25. The wear track after abrasion test a) not alloyed austenitic stainless steel surface and b) duplex stainless steel alloyed with SiC, surface with 3 grooves of 0.5 mm

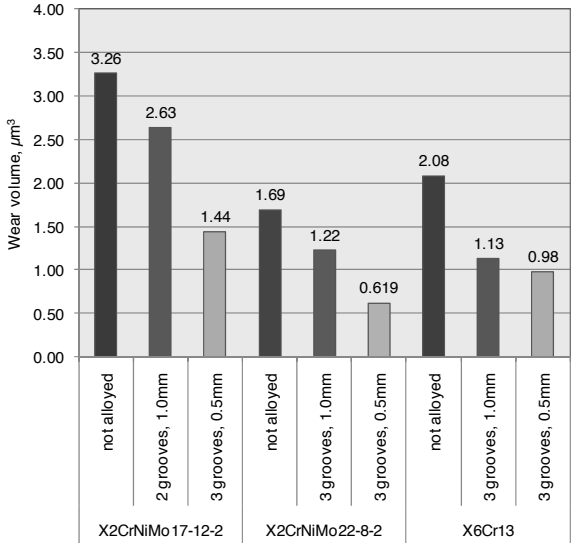

Fig. 26. Abrasive wear behaviour of laser alloyed SiC layer (wear test: 5.0 mm diameter hardened steel ball, load 7.4 kN, reciprocal sliding movement, path of friction 7 mm, constant 9000 cycles)

Samples with 3 grooves shows higher wear resistance in respect to samples with 2 grooves but their microhardness is slightly lower and more inform distributed along the depth profile. Abrasion mechanism in this case seams to be in favour of a uniform microstructure obtained for 3 grooves of 0.5 mm than slightly harder surface but on less depth. If on the surface are presented hard silicon particles that divert from the surface during sliding they may act as abrasive particles and thus increase wear volume of harder alloyed layers. In term of wear resistance the lower wear volume was obtained for alloyed duplex stainless steel. Improvement of wear resistance of alloyed duplex stainless steel is connected with increase of hardness due to ferrite content increase, fine microstructure formed by high cooling rates of laser processing and dissolution of silicon and carbon in the alloy matrix as well as presence of formed precipitates like silicates and carbides and SiC particles.

FEM simulation model

The FEM computations were performed using ANSYS software. The scope of FEM simulation was determination of temperature distribution during laser alloying process at various process configurations regarding laser beam power and method of powder deposition, as pre coated past or surface with machined grooves. The FEM simulation was performed on five different 3-dimesional models. The model assumed non linear change of thermal conductivity, specific heat and density that were depended on temperature. The finite element mesh was created with the 20-noded thermal Solid90 elements. The element has a single degree of freedom, the temperature at each node. The heating process was realized as heat flux corresponding to laser beam power of 0.7, 1.4 and 2.1 kW, while heat removal as radiation and convection of 800 J/kg. Latent heat effects are considered during solidification. The molten pool is composed of the same material as the substrate and there is no chemical reaction between alloying material and base metal. The simulation included different materials properties of base metal as well as alloying SiC powder. The initial sample temperature and room temperature was the same, 293 K. The assumed surface emissivity was 0.95. The laser beam was incident perpendicularly to the base metal and the energy was assumed to be distributed uniformly in a rectangular area of 6.8 mm × 1.8 mm. The absorptivity of laser energy was dependent on the simulated materials properties and their surface condition of the base metal and feed materials. The laser movement along alloyed surface was simulated, and set to 0.3 or 0.5 m/min.

The FEM simulation allows specifying the heat affected zone and the temperature distribution in the sample as a function of time and thus allows the estimation of the structural changes taking place during laser alloying process (Fig. 27). The simulation was applied to determine the shape of molten pool and the penetration depth of alloying surface. The penetration depth was measured from the end of surface layer towards the depth basing on the temperature of melting metal, where as the final penetration depth was accepted the temperature melting temperature (Fig. 28). The possibly cladding material on the surface as well as shrinkage of molten pool during solidification was not taken into consideration. Basing on this assumption the penetration depth of alloyed layer can be easy calculated. Fig. 28 shows 3 different simulations dependent on elaborated 3-dimensional model.

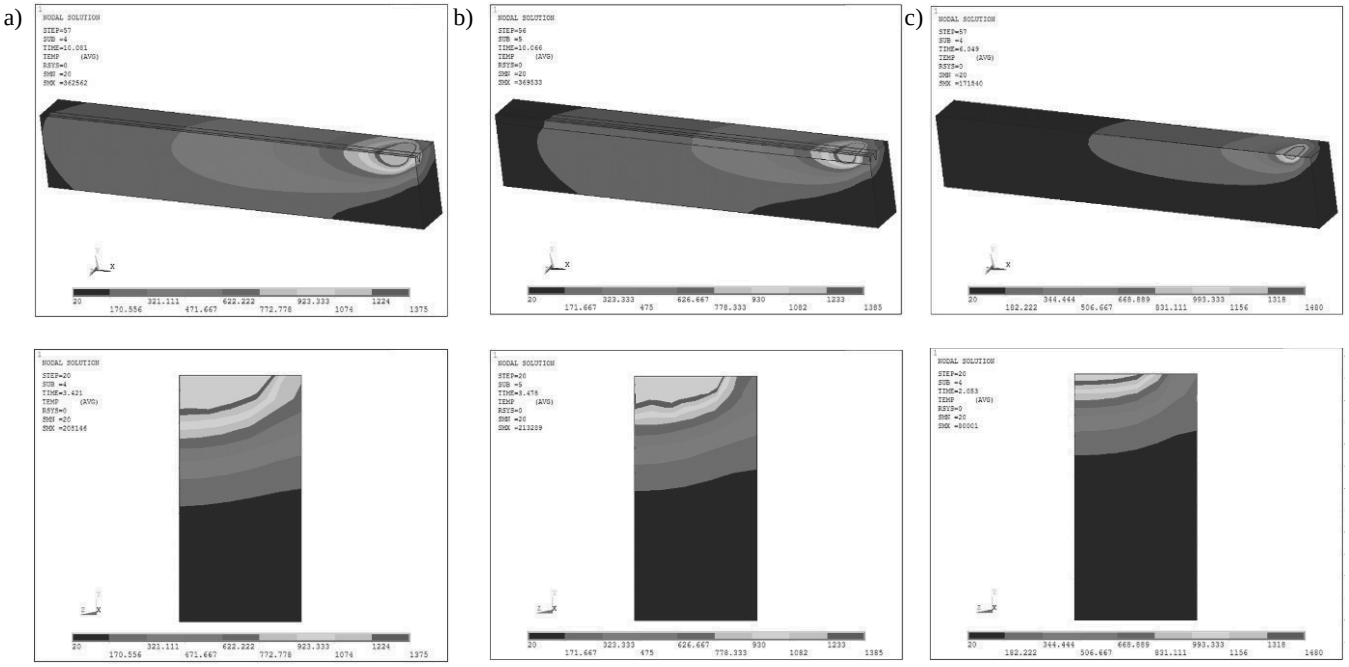

Fig. 27. The spatial distribution of temperature in a cross-section of sample during laser alloying with SiC powder, a) austenitic stainless X2CrNiMo17-12-2, laser beam power 2.1 kW, scanning speed 0.3 m/min, surface with machined 2 grooves of 1.0 mm; b) duplex stainless steel X2CrNiMo22-8-2, laser beam power 2.1 kW, scanning speed 0.3 m/min, surface with machined 3 grooves of 1.0 mm; c) ferritic stainless steel laser beam power 2.1 kW, scanning speed 0.5 m/min, powder deposited as pre-coated paste

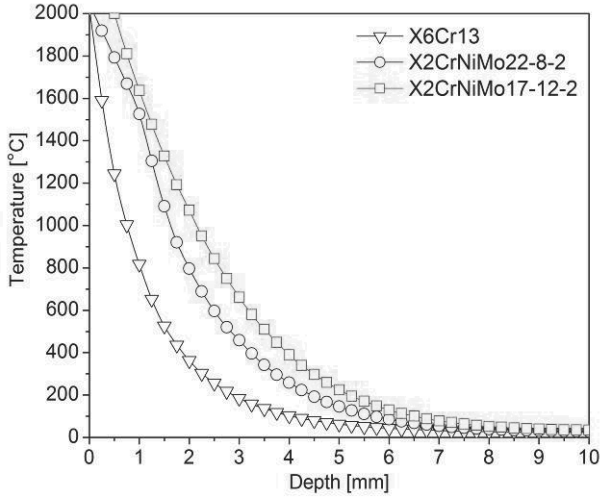

Fig. 28. The temperature changes in function of sample depths during laser alloying with SiC, ferritic stainless steel X6Cr13, laser beam power of 2.1 kW, scanning speed 0.5 m/min, powder deposited as pre-coated paste; duplex stainless steel X2CrNiMo22-8-2, laser beam power 2.1 kW, scanning speed 0.3 m/min, surface with machined 3 grooves of 1.0 mm; austenitic stainless steel X2CrNiMo17-12-2, laser beam power 2.1 kW, scanning speed 0.3 m/min, surface with machined 2 grooves of 1.0 mm

Simulated penetration depth and molten pool profile good mach the experimental results. The depth values obtained in simulation are very close to experimental data (Fig. 29). Regarding the shape of molten pool the little differences have been noted. The heat flux input considered in simulation is only part of the mechanism for heating, thus the final shape of solidified molten pool will be depended of more variables.

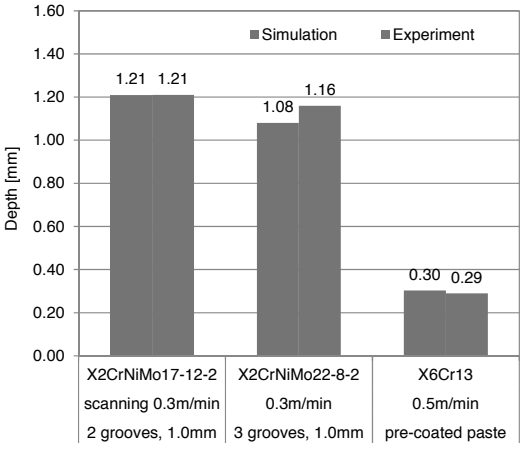

Fig. 29. Comparison of experimental and simulated penetration depth of surface alloyed with SiC at laser beam power 2.1 kW for various materials and processing conditions

4. Conclusions

On the basis of the above experimental results of the study concerning to investigation of the laser alloying with SiC of sintered stainless steels, the following conclusions can be summarised:

a) The powder deposition method plays an important role in obtained materials microstructures and properties. Surfaces prepared with pre-coated paste shows lover quality than prepared as machined grooves. Machined grooves filled with alloyed powder gives possibilities to control the quantity of remelted material and dilution ratio.
b) Increase of laser beam power resulted in slight widening of remelting zone and more remarkable on the penetration depth. Beside evaluated materials the austenitic X2CrNiMo17-12-2 shows highest penetration depth ca. 0.9 mm, while for duplex it was ca. 0.6 mm and only 0.2-0.3 for ferritic stainless steel.
c) Surface with grooves filed with alloying powder SiC ensure better remelting surface quality than surface covered with pre-coated powder paste that acts as the barrier for laser radiation and lowers possible penetration depth. The surface quality when SiC was deposited as pre-coated paste it was satisfactory for ferritic and austenitic stainless steels after laser alloying, but in case of duplex stainless steel and low laser beam powers the superficial porosities where drastically higher.
d) The microstructure of austenitic stainless steels remelted with SiC powder is composed of primary dendrites of austenite phase and interdendritic lamellar eutectics of austenite and carbides M_7C_3 (M = Cr, Fe). The ferritic stainless steel shows fine dendritic structure, where central zone of remelted layer is composed of very fine and regularly distributed dendrites and precipitations of silicides and flower-shaped carbides which predominateed at the top of alloyed layer. The duplex stainless steel microstructure contains the mixture of austenite, ferrite, silicides and carbon precipitations.
e) The dissolution of SiC phases during lassser alloying leads to the formation of phases such as carbides M_7C_3 type, SiC phase, silicon rich phases as FeSi, Fe_3Si as well as $C_{0.12}$ $Fe_{0.79}$ $Si_{0.09}$ phase depending on the dilution ratio of alloyed layer.
f) The infrared thermography can be usefully applied to determination of temperature distribution during laser alloying and can be helpful in understanding the phenomena occurring during this process.
g) The laser alloyed surface hardening effect is caused by precipitation of silicedes and hard carbides, dissolution of Si and C in alloy matrix as well as complete reduction of porosity, Samples with pre-coated paste shows high superficial hardness due to not dissolved SiC particles on the surface, this effect was strongest in ferritic stainless steel where microhardness increased to $1200HV_{0.1}$ for 1.4 kW. Subsequent increase of laser beam power resulted in lowering of microhardness to ca. $850HV_{0.1}$ for 2.1 kW, due to higher dissolution of substrate material. Beside studied stainless steels where in surface grooves were machined the duplex stainless steels revealed highest microhardness about 500-600HV.
h) The laser alloyed layers produced on the surface with machined grooves demonstrated a significant improvement of wear resistance comparing to not alloyed layer. The highest wear resistance was obtained for duplex stainless steel.
i) Simulated be FEM penetration depth and molten pool shape mach the experimental results.

Laser surface alloying with SiC powder can be an efficient method of surface layer hardening of sintered stainless steels and produce significant improvement of surface layer properties in terms of hardness and wear resistance. Moreover, application of high power diode laser HPDL and surface prepared as machined grooves can guarantee uniform heating of treated surface, thus uniform thermal cycle across processed area and uniform penetration depth of alloyed surface layer.

Acknowledgements

The presented research was partially funded by the Polish Ministry of Science and Higher Education as a research project No. N507 470137.

References

[1] C. Tassin, F. Laroudie, M. Pons, L. Lelait, Improvement of the wear resistance of 316L stainless steel by laser surface alloying, Surface and Coatings Technology 80 (1996) 207-210.
[2] J.C. Betts, The direct laser deposition of AISI316 stainless steel and Cr_3C_2 powder, Journal of Materials Processing Technology 209 (2009) 5229-5238.
[3] F. Laroudie, C. Tassin, M. Pons, Hardening of 316L stainless steel by laser surface alloying, Journal of Materials Science 30 (1995) 3652-3657.
[4] D. Zhang, X. Zhang, Laser cladding of stainless steel with Ni-Cr_3C_2 and Ni-WC for improving erosive-corrosive wear performance, Surface and Coatings Technology 190 (2005) 212-217.
[5] J. Dutta Majumdar, I. Manna, Laser surface alloying of AISI304-stainless steel with molybdenum for improvement in pitting and erosion-corrosion resistance, Materials Science and Engineering A 267 (1999) 50-59.
[6] C.T. Kwok, F.T. Cheng, H.C. Man, Laser surface modification of UNS S31603 stainless steel, Part I, Microstructures and corrosion characteristics, Materials Science and Engineering A 290 (2000) 55-73.
[7] S. Zherebtsov, K. Meakawa, T. Hayashi, M. Futakawa, Laser surface alloying of SUS316 stainless steel with Al-Si, JSME International Journal A 48/4 (2005) 292-298.
[8] L.A. Dobrzański, M. Bonek, E. Hajduczek, K. Labisz, M. Piec, E. Jonda, A. Polok, Structure and properties of laser alloyed gradient surface layers of the hot-work tool steel, Journal of Achievements in Materials and Manufacturing Engineering 31/2 (2008) 148-169.
[9] L.A. Dobrzański, S. Malara, T. Tański, Laser surface treatment of magnesium alloys with silicon carbide powder, Archives of Materials Science and Engineering 35/1 (2009) 54-60.

[10] A. Lisiecki, A. Klimpel, Diode laser surface modification of Ti6Al4V alloy to improve erosion wear resistance, Archives of Materials Science and Engineering 32/1 (2008) 5-12.
[11] F. Yongquing, A.W. Batchelor, Laser alloying of aluminum alloy AA6061 with Ni and Cr, Part II, The effect of laser alloying on the fretting wear resistance, Surface and Coatings Technology 102 (2003) 468-471.
[12] Sang-Zoon Leea, K.-H. Zum Gahra, Laser-induced surface alloying of Al2O3 ceramics with ZrO2-TiO2 powders, Ceramics International 20/3 (1994) 147-157.
[13] A. Dudek, Z. Nitkiewicz, A. Górka, Structure and properties of laser alloyed surface layer, Journal of Achievements in Materials and Manufacturing Engineering 27/1 (2008) 75-78.
[14] W. Ozgowicz, A. Kurc, Structure and properties of forming austenitic X5CrNi18-9 stainless steel in a cold working, Journal of Achievements in Materials and Manufacturing Engineering 33/1 (2009) 19-26.
[15] G. Niewielski, K. Radwański, D. Kuc, The impact of deformation on structural changes of the duplex steel, Journal of Achievements in Materials and Manufacturing Engineering 23/1 (2007) 31-34.
[16] A. Baron, W. Simka, G. Nawrat, D. Szewieczek, Electropolishing and chemical passivation of austenitic steel, Journal of Achievements in Materials and Manufacturing Engineering 31/2 (2008) 197-202.
[17] W.S. Lin, The study of high speed fine turning of austenitic stainless steel, Journal of Achievements in Materials and Manufacturing Engineering 27/2 (2008) 191-194.
[18] Z. Brytan, L.A. Dobrzański, M. Actis Grande, M. Rosso, Characteristics of vacuum sintered stainless steels, Journal of Achievements in Materials and Manufacturing Engineering 33/2 (2009) 126-134.
[19] Z. Brytan, M. Actis Grande, M. Rosso, R. Bidulský, L.A. Dobrzański, Stainless steels sintered form the mixture of prealloyed stainless steel and alloying element powders, Materials Science Forum 672 (2011) 165-170
[20] Z. Brytan, M. Bonek, L.A. Dobrzański, Microstructure and properties of laser surface alloyed PM austenitic stainless steel, Journal of Achievements in Materials and Manufacturing Engineering 40/1 (2010) 70-78.
[21] S. Buytoz, Microstructural properties of SiC based hard facing on low alloy steel, Surface and Coatings Technology 200 (2006) 3734-3742.
[22] S. Buytoz, M. Ulutan, In situ synthesis of SiC reinforced MMC surface on AISI304 stainless steel by TIG surface alloying, Surface and Coatings Technology 200 (2006) 3698-3704.
[23] C.T. Kwok, K.I. Leong, F.T. Cheng, H.C. Man, Microstructural and corrosion characteristics of laser surface-melted plastics mold steels, Materials Science and Engineering A 357 (2003) 94-103.
[24] G. Thawari, G. Sundararajan, S.V. Joshi, Laser surface alloying of medium carbon steel with $SiC_{(P)}$, Thin Solid Films 423 (2003) 41-53.
[25] F. Laroudie, C. Tassin, M. Pons, Hardening of 316L stainless steel by laser surface alloying, Journal of Materials Science 30 (1995) 3652-3657.